GEOLOGY | THE GEOLOGICAL SOCIETY OF AMERICA®

https://doi.org/10.1130/G49206.1

Manuscript received 29 April 2021
Revised manuscript received 29 June 2021
Manuscript accepted 29 June 2021

Published online 30 August 2021

Active faulting controls bedform development on a deep-water fan

Vittorio Maselli[1], Aaron Micallef[2,3], Alexandre Normandeau[4], Davide Oppo[5], David Iacopini[6], Andrew Green[7] and Zhiyuan Ge[8]

[1]Department of Earth and Environmental Sciences, Dalhousie University, Halifax, Nova Scotia B3H 4R2, Canada
[2]Marine Geology and Seafloor Surveying, Department of Geosciences, University of Malta, Msida 1805, Malta
[3]Helmholtz Centre for Ocean Research, GEOMAR, 24148 Kiel, Germany
[4]Geological Survey of Canada, Natural Resources Canada, Dartmouth, Nova Scotia B2Y 4A2, Canada
[5]School of Geosciences, University of Louisiana at Lafayette, Lafayette, Louisiana 70504, USA
[6]DiSTAR (Department of Earth, Environmental and Resources Sciences), Università di Napoli Federico II, 80138 Naples, Italy
[7]Geological Sciences, University of KwaZulu-Natal, Durban 4041, South Africa
[8]College of Geosciences, China University of Petroleum, Beijing 94305, China

ABSTRACT

Tectonically controlled topography influences deep-water sedimentary systems. Using 3-D seismic reflection data from the Levant Basin, eastern Mediterranean Sea, we investigate the spatial and temporal evolution of bedforms on a deep-water fan cut by an active normal fault. In the footwall, the fan comprises cyclic steps and antidunes along its axial and external portions, respectively, which we interpret to result from the spatial variation in flow velocity due to the loss of confinement at the canyon mouth. Conversely, in the hanging wall, the seafloor is nearly featureless at seismic scale. Numerical modeling of turbidity currents shows that the fault triggers a hydraulic jump that suppresses the flow velocity downstream, which thus explains the lack of visible bedforms basinward. This study shows that the topography generated by active normal faulting controls the downslope evolution of turbidity currents and the associated bedforms and that seafloor geomorphology can be used to evince syn-tectonic deposition.

INTRODUCTION

Deep-water fans form the largest sediment accumulations on Earth (Menard, 1955; Jobe et al., 2018) and are archives of past tectonic and climatic events (Blum et al., 2018). Deep-water fans are primarily fed and shaped by turbidity currents, which are sediment-laden turbulent flows that move down subaqueous slopes under gravity (Meiburg and Kneller, 2010) and globally represent the dominant mechanism for transporting sediment, organic matter, and pollutants from continents to the deep sea (e.g., Zhong and Peng, 2021).

Turbidity currents reaching a supercritical status (i.e., densimetric Froude number [Fr] > 1) form bedforms that are considered to be building blocks of deep-water depositional systems (Covault et al., 2017). These bedforms are thought to be responsible for the inception of new slope channels and canyons (Fildani et al., 2013); they shape channel-lobe transition zones and fans (Postma et al., 2016) and focus the accumulation of plastic litter at the seafloor (Zhong and Peng, 2021). Deep-water fans are dissected by a variety of erosional and depositional features, which are often interpreted as upper flow regime bedforms, such as antidunes and cyclic steps (Wynn and Stow, 2002; Fildani et al., 2006; Normandeau et al., 2019; Maier et al., 2020). While antidunes are formed by supercritical turbidity currents (Fr > 1), cyclic steps are related to transcritical flows, as each step is bounded at its upstream and downstream end by a hydraulic jump, which is a short zone over which the flow experiences a rapid transition from shallow and supercritical (Fr > 1) to thick and subcritical (Fr < 1) (Parker and Izumi, 2000; Fildani et al., 2006; Cartigny et al., 2011; Kostic, 2011). It has been proposed that seafloor rugosity, either generated internally (Guiastrennec-Faugas et al., 2020; Heijnen et al., 2020) or caused by external factors (Ercilla et al., 2002; Covault et al., 2014; Maier et al., 2017), controls the velocity of (near) supercritical and transcritical flows and thus promotes the formation of antidunes and cyclic steps (Cartigny et al., 2014). Fault topography is known to influence turbidite deposition at the fan-scale (Ge et al., 2017, 2018), but the control of active tectonics on turbulent gravity flows and associated bedforms is poorly known. For example, it is unclear how the vertical displacement of an active normal fault, which we term a dynamic knickpoint, influences sediment deposition through supercritical and transcritical turbidity currents and how bedforms record this influence.

We integrated 3-D seismic reflection data with numerical modeling to show how a dynamic knickpoint influences sediment deposition on a deep-water fan in the Levant Basin (Fig. 1; eastern Mediterranean Sea). By investigating the interaction between active faulting and sediment transport processes, we provide new insights into the influence of autogenic and allogenic forcing factors on turbidite deposition, which has important implications for understanding how tectonic signals are preserved in the depositional record.

GEOLOGICAL SETTING

The Miocene to recent stratigraphy of the Levant Basin is characterized by evaporites overlain by up to 1.5 km of clastic deposits (Oppo et al., 2021). Tectonic forces and differential sediment loading led to the deformation and basinward movement of the evaporites (Allen et al., 2016) and generated margin-parallel, salt-detached growth faults (Fig. 2). The presence of fault escarpments at the seafloor (Figs. 1A

CITATION: Maselli, V., et al., 2021, Active faulting controls bedform development on a deep-water fan: Geology, v. 49, p. 1495–1500, https://doi.org/10.1130/G49206.1

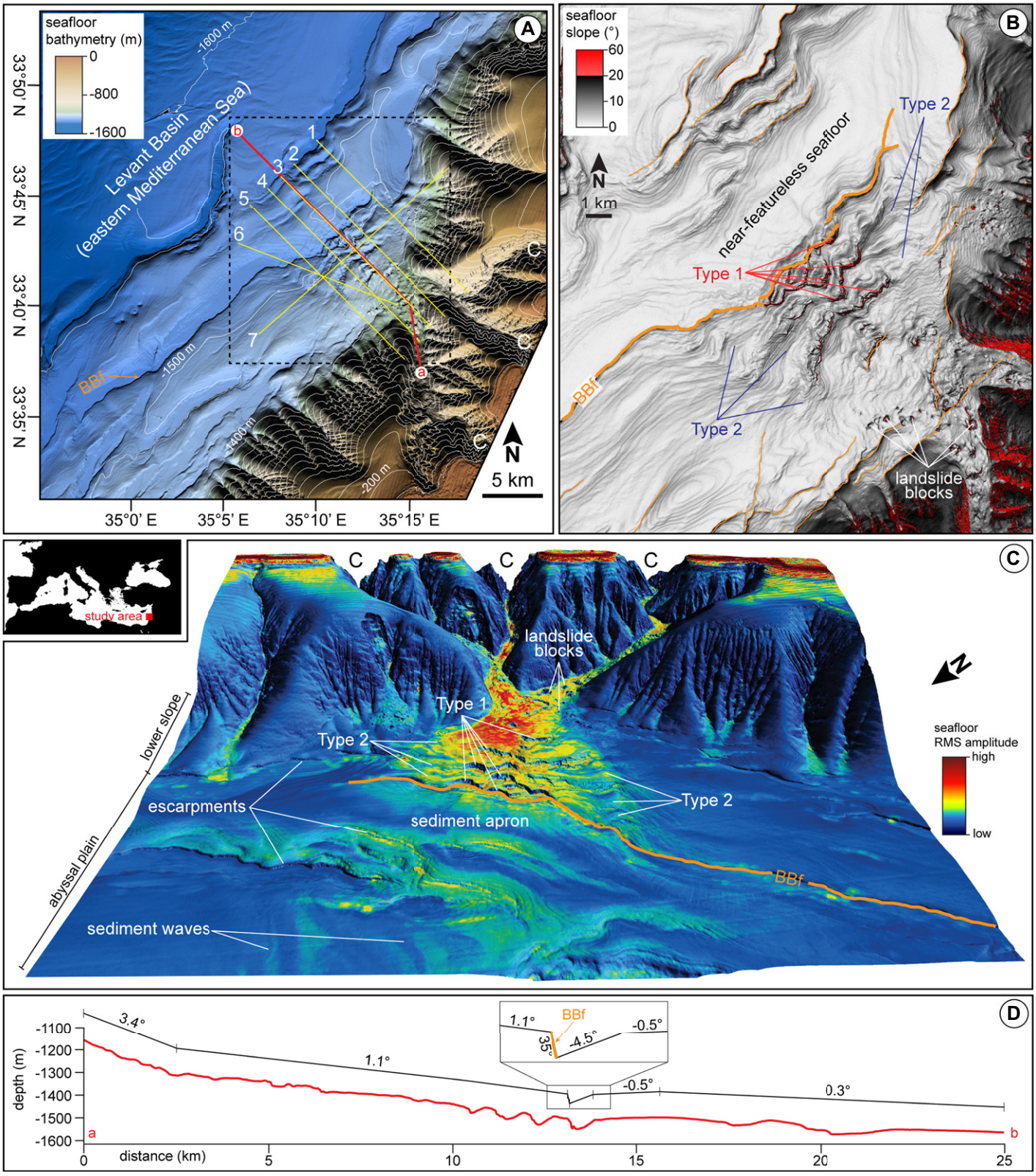

Figure 1. (A) Bathymetry of the study area, in 100-m-spaced contours. Dashed rectangle outlines map in B; yellow lines (1–7) indicate locations of seismic profiles in Figure 2; red line marks the bathymetric section in D. BBf—Bedform Bounding fault; C—Canyons. (B) Seafloor slope with fault escarpments (orange) and the BBf. (C) Three-dimensional view of the seafloor with root-mean-square (RMS) amplitude attribute. (D) Red line indicates bathymetric section a-b in A; black line shows the simplified section used in the numerical modeling.

and 1B; and side-scan sonar images of Elias et al. [2007]) indicates that fault movement is still ongoing.

DATA AND METHODS

We interpreted 1650 km^2 of 3-D, post-stack Kirchhoff, time-migrated seismic reflection data (Fig. 1). The dominant frequency within 50 ms below seafloor is ~90 Hz, and the vertical resolution is ~4.5 m assuming a P-wave velocity of

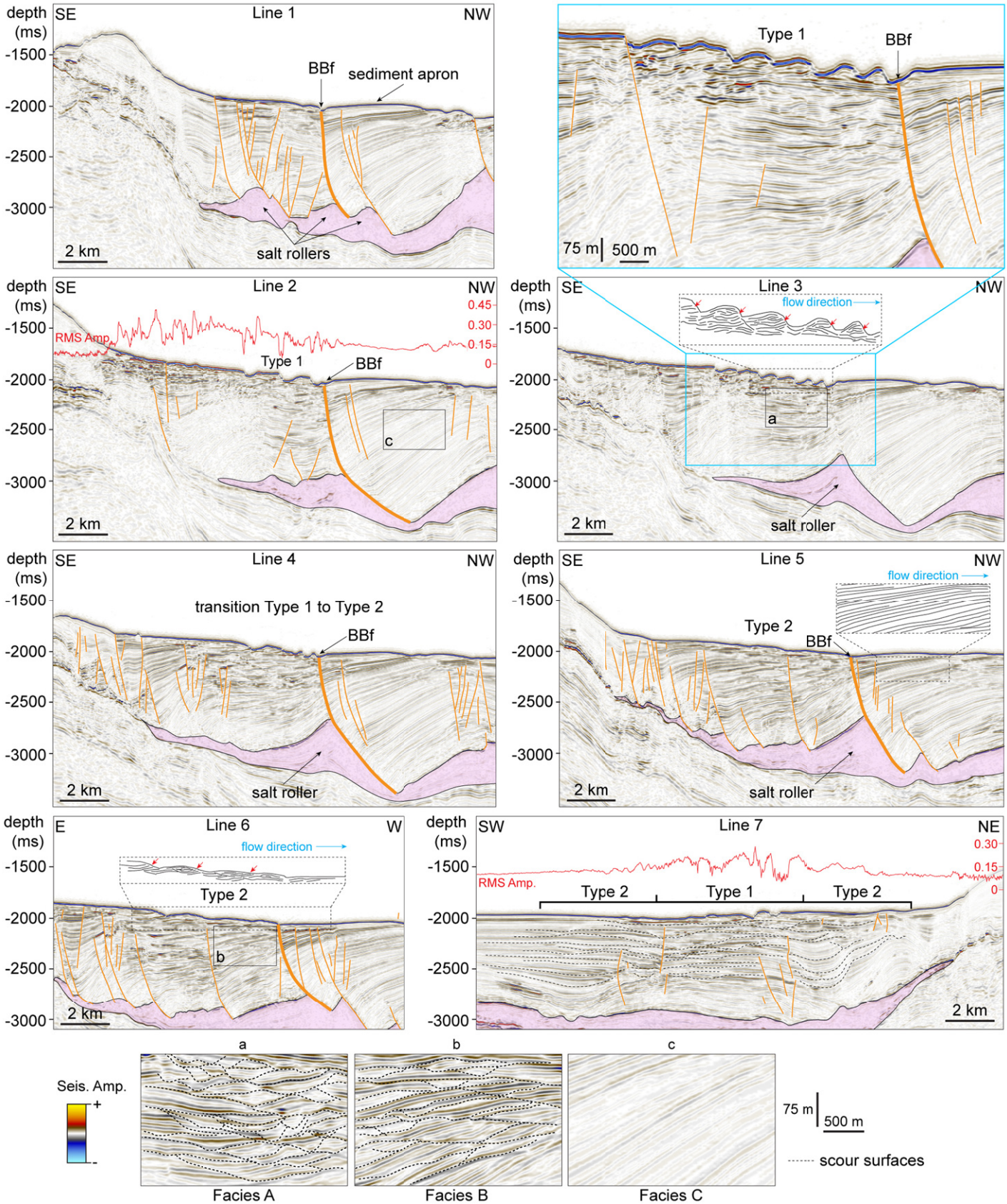

Figure 2. Seismic profiles (location in Fig. 1A) show faults in orange (thicker line for the Bedform Bounding fault [BBf]) and salt deposits in pink; blue square gives a close-up view of line 3. Line drawings of the internal stratigraphy of type 1 and 2 bedforms are presented for lines 3 and 6, respectively, which are indicated by dashed rectangles; red arrows point to the truncation of reflections; black squares (a–c) mark the locations of the close-up views used to describe seismic facies (A to C); red curves in lines 2 and 7 are extractions of the root-mean-square (RMS) seismic amplitude along the seismic profile and are scaled from 0 to 1.

1600 m/s. The bathymetry was derived by picking the first reflection and is presented at a scale of 25 m × 25 m. Visibility, sensu Brown (2011), extends the ability to see geological features on this surface to ~10 m. The uncertainty in the calculation of seafloor gradients is 5%–10%. We used a velocity of 1500 m/s for time to depth conversion of the seafloor surface. Since seabed sediment sampling is lacking, we used the root-mean-square (RMS) amplitude attribute of the seafloor reflection as a proxy for sediment grain size, with high amplitude indicating coarser deposits, as suggested in other studies (Chen and Sidney, 1997; Maselli et al., 2019).

We also conducted a series of numerical simulations of turbidity currents running on a simplified topography derived from a bathymetric section along the fan axis (Figs. 1A and 1D). The model uses Reynolds-Averaged Navier–Stokes (RANS) methods with k – ε Renormalization Group (RNG) turbulence to simulate the control of the fault throw and seafloor slope on the hydraulic and depositional/erosional processes of turbidity currents (see Section S1 in the Supplemental Material[1]). Based on constraints from Covault et al. (2014), the flow is 15 m thick with an initial velocity of 1.5 m/s and sediment concentration of 0.4% (0.1% silt, 0.2% very fine sand, 0.1% fine sand). These values are consistent with field data from the La Jolla Fan (southern California; Maier et al., 2020), where muddy sediments are interbedded with well-sorted sands, and the Congo Canyon (west Africa; Simmons et al., 2020), where dilute flows (<10 g/l) have been captured at ~2000 m water depth (w.d.).

RESULTS

Seafloor Bathymetry and Seismic Amplitude Response

In the study area, three shelf-incising canyons merge at the base of the slope and feed a deep-water fan (Fig. 1). The canyons' thalwegs have a gradient of ~3.7°, which sharply decreases to ~1.2° at ~1400 m w.d. (Section S2 in the Supplemental Material). This change in gradient marks the landward limit (i.e., apex) of the fan. Landslide blocks are widespread within the lower reaches of the canyons (Fig. 1B). Northwest-dipping and southwest-northeast–striking elongate escarpments represent the seafloor expression of normal faults (Fig. 1) as shown in seismic profiles (Fig. 2). The main growth fault within the study area, which we name the Bedform Bounding fault (BBf), generates a 35-km-long and up to 18-m-high fault escarpment at the seafloor, which dips at 35° seaward (Figs. 1 and 2).

The fan is characterized by seafloor gradients of ~1.2° and ~0.2° landward and seaward of the BBf, respectively. In the footwall of the BBf, two types of bedforms are visible at the seafloor: type 1 in the axial fan section, and type 2 on its external portions (Fig. 1B). Type 1 bedforms are crescentic in shape, 35–50 m high and 830–1465 m long, and have an aspect ratio of ~30. In cross section, the bedforms are asymmetric and have lee and stoss side gradients of 12.2°–23.7° and 4.1°–6.4°, respectively (Fig. 1); these values decrease in an upslope direction (Section S3 in the Supplemental Material). The escarpment of the BBf is also partially reworked by coalescent type 1 bedforms (Section S4 in the Supplemental Material). Type 2 bedforms have slightly sinuous crests and are 5–30 m high and 910–1670 m long (Fig. 1), which gives an aspect ratio >50. In cross section, the bedforms are asymmetric with lee and stoss side gradients of 7.3°–2.6° and 3.6°–0.5°, respectively (Section S3 in the Supplemental Material). The BBf marks a sharp transition from the bedform fields to a seismically featureless seafloor in the nearest 4 km seaward of the BBf (Fig. 1). This region has an overall convex-up morphology (Fig. 2; Section S4 in the Supplemental Material), which corresponds to a sediment apron (Fig. 2, line 1; Section S5 in the Supplemental Material). Farther basinward, a new series of sediment waves with kilometer-scale wavelength, visible in the RMS map (Fig. 1C), develops where there is an increase in seafloor slope to ~0.6° (Section S6 in the Supplemental Material).

Seafloor RMS amplitude is low across much of the slope and abyssal plain, whereas high values occur along the canyons and on the fan at the footwall of the BBf (Fig. 1C). Intermediate amplitude values are visible across the landward-facing side of the sediment apron (Fig. 1C). RMS amplitude values extracted along two seismic sections oriented perpendicular and parallel to the slope across the fan (Fig. 2, lines 2 and 7, respectively) show sharp changes on the fan when crossing the erosional side of type 1 bedforms, on the escarpment related to the BBf, and on landslide blocks that are visible at the seafloor (Figs. 1B and 1C; Section S6 in the Supplemental Material). Overall, the RMS values gradually decrease basinward across the fan (Fig. 2).

Seismic Facies and Geometry

Where type 1 bedforms are present (Fig. 2, lines 2 and 3), seismic reflections are wavy to hummocky with alternating high and low amplitudes (Fig. 2, facies A). Seismic packages are separated by multiple erosional surfaces, which are also wavy. Truncated reflections, which dip landward, are visible on the lee side of type 1 bedforms at the seafloor (Fig. 2; see red arrows in line 3). Where type 2 bedforms are present (Fig. 2, lines 5 and 6), seismic reflections are undulating to subparallel, dip landward, and form alternating high- and low-amplitude packages, which are separated by linear to undulating erosional surfaces that dip landward (Fig. 2, facies B). Truncated reflections, which also dip landward, are visible on the lee side of type 2 bedforms at the seafloor (Fig. 2; see red arrows in line 6). The transition from seismic facies A to B, which also corresponds to the change from type 1 to type 2 bedforms at the seafloor, is clearly visible on a section oriented perpendicular to the main slope direction (Fig. 2, line 7).

On the hanging wall of the BBf, seismic packages thin seaward and are characterized by low-amplitude continuous, inclined to divergent, reflections (Fig. 2, line 1), and alternate with higher amplitude reflections (Fig. 2, facies C). Seismic facies change abruptly from A to C at the BBf fault (Fig. 2, lines 1–6). The overall wedge-shaped geometry of seismic strata indicates syn-depositional growth associated with normal fault activity.

DISCUSSION

Interpretation of Inferred Flow Properties from Bedforms

We interpret type 1 bedforms as partially depositional cyclic steps because of >10° dipping lee and stoss sides, erosional lee sides, and backstepping stratigraphy, and type 2 as antidunes because of gentler gradients, larger aspect ratio, and reduced lee side erosion (Slootman and Cartigny, 2020). Cyclic steps and antidunes coexist at the seafloor (Fig. 1C) and make up the stratigraphy of the fan; vertically stacked and upslope migrating cyclic steps and antidunes accumulate on the axial and external portions, respectively (Fig. 2). The coexistence of cyclic steps and antidunes landward of the BBf suggests that the flows are supercritical to transcritical on the fan. We argue that the flow relaxation due to loss of confinement at the canyon mouth generates spatial variation in the flow velocity of the turbidity currents, which is responsible for the synchronous deposition of the two types of bedforms: a higher flow velocity in the axial fan generates cyclic steps, whereas a lower velocity at the sides forms antidunes. Such flow relaxation mechanism has been reproduced in flume tank experiments, which suggests that turbidity currents, when exiting from a confined system, may experience higher flow velocity along the axial portion, where bed erosion may occur due to an increase in basal shear stress (Pohl et al., 2019).

RMS amplitude response, and thus the inferred sediment grain size, is highest where cyclic steps are located, lowest outside the fan, and intermediate where antidunes are present. Flume tank experiments indicate that cyclic steps in

[1]Supplemental Material: Additional information about the numerical modeling, bathymetric profiles, cross sections along type 1 and type 2 bedforms, a 3-D view of the study area, seafloor bathymetry and thickness map of post-salt deposits, and morphology of sediment waves seaward of the fan. Please visit https://doi.org/10.1130/GEOL.S.15138618 to access the supplemental material, and contact editing@geosociety.org with any questions.

fine sand develop considerably steep lee sides (Cartigny et al., 2014), which agrees with the 24° dipping lee faces we observe in type 1 bedforms (cyclic steps).

Influence of a Dynamic Knickpoint on Turbidity Currents

The disappearance of bedforms and the decrease in seafloor gradient from ~1.2° to ~0.2° across the BBf indicate that the fault has had a dominant control on the behavior of turbidity currents and the sedimentological properties and geometry of the fan. Modeling results of a turbidity current show that the flow is supercritical over the fan and that the knickpoint formed by the BBf triggers a larger hydraulic jump at its base, which reduces flow velocity and Froude number and hampers the development of visible bedforms seaward of the fault (Fig. 3).

The formation of hydraulic jumps in turbidity currents due to seafloor irregularities, either generated by tectonics or mass-transport deposits, has been investigated in different settings (Ercilla et al., 2002; Covault et al., 2014; Ge et al., 2017; Howlett et al., 2019). Our results indicate that sedimentary bedforms may record the interaction between turbidity currents and topography generated by active faulting at the seafloor (i.e., a dynamic knickpoint) and thus can help to quantify intervals of syn-tectonic deposition in the stratigraphic record. We show that tectonically induced rugged topography may suppress supercritical to transcritical flows and thus influence the distribution of sedimentary facies within the fan, which has important implications for reservoir properties in tectonically active settings and for the sequestration of land-derived material in the deep ocean.

The reduced seafloor gradient in the hanging wall (~0.2°) could also control the transition to a Froude subcritical flow and thus explain the lack of visible bedforms, as discussed by Zhong et al. (2015). Recent studies from offshore California based on bathymetric data with (sub)meter-scale resolution, however, have shown that small-scale bedforms can be widespread over the surface of deep-water fans, which suggests that supercritical and transcritical flows may still develop in low-gradient settings for a given flow depth and sediment concentration (Maier et al., 2020; Fildani et al., 2021).

CONCLUSION

Our study shows that deep-water fans are sculpted into supercritical and transcritical bedforms and that the topography generated by active normal faulting triggers a hydraulic jump that suppresses the flow velocity of turbidity currents downstream and thus hampers bedform development and influences facies distribution. This outcome has two key implications: (1) the nature and distribution of bedform fields can be used to quantify intervals of syn-tectonic deposition in the stratigraphic record, which thus supports the interpretation of turbidite fans in other active settings such as rifted margins and salt-dominated basins; and (2) sediments, and associated organic matter and anthropogenic pollutants, are vigorously transported into the deepest reaches of the oceans. Our results also indicate that the loss of confinement at the canyon mouth can generate spatial variation in the flow velocity of the turbidity currents (i.e., flow relaxation) and lead to the synchronous deposition of antidunes and cyclic steps.

ACKNOWLEDGMENTS

We thank Wissam Chbat and the Lebanese Petroleum Administration for data access and for allowing publication of this work, and Schlumberger for granting Petrel academic licenses. We are grateful to editor Gerald Dickens, and to Andrea Fildani, Matthieu Cartigny, and an anonymous reviewer for suggestions that greatly improved the manuscript. V. Maselli acknowledges support from the Natural Sciences and Engineering Research Council of Canada Discovery Grant (RGPIN-2020–04461). A. Micallef acknowledges support from the Horizon 2020 European Research Council program (677898, MARCAN).

REFERENCES CITED

Allen, H., Jackson, C.A.-L., and Fraser, A.J., 2016, Gravity-driven deformation of a youthful saline giant: The interplay between gliding and spreading in the Messinian basins of the Eastern Mediterranean: Petroleum Geoscience, v. 22, p. 340–356, https://doi.org/10.1144/petgeo2016-034.

Blum, M., Rogers, K., Gleason, J., Najman, Y., Cruz, J., and Fox, L., 2018, Allogenic and autogenic signals in the stratigraphic record of the deep-sea Bengal Fan: Scientific Reports, v. 8, 7379, https://doi.org/10.1038/s41598-018-25819-5.

Brown, A.R., 2011, Interpretation of Three-Dimensional Seismic Data, 7th edition: Tulsa, Oklahoma, Society of Exploration Geophysicists, 646 p.

Cartigny, M.J.B., Postma, G., van Den Berg, J.H., and Mastbergen, D.R., 2011, A comparative study of sediment waves and cyclic steps based on geometries, internal structures and numerical modeling: Marine Geology, v. 280, p. 40–56, https://doi.org/10.1016/j.margeo.2010.11.006.

Cartigny, M.J.B., Ventra, D., Postma, G., and van Den Berg, J.H., 2014, Morphodynamics and sedimentary structures of bedforms under supercritical-flow conditions: New insights from flume experiments: Sedimentology, v. 61, p. 712–748, https://doi.org/10.1111/sed.12076.

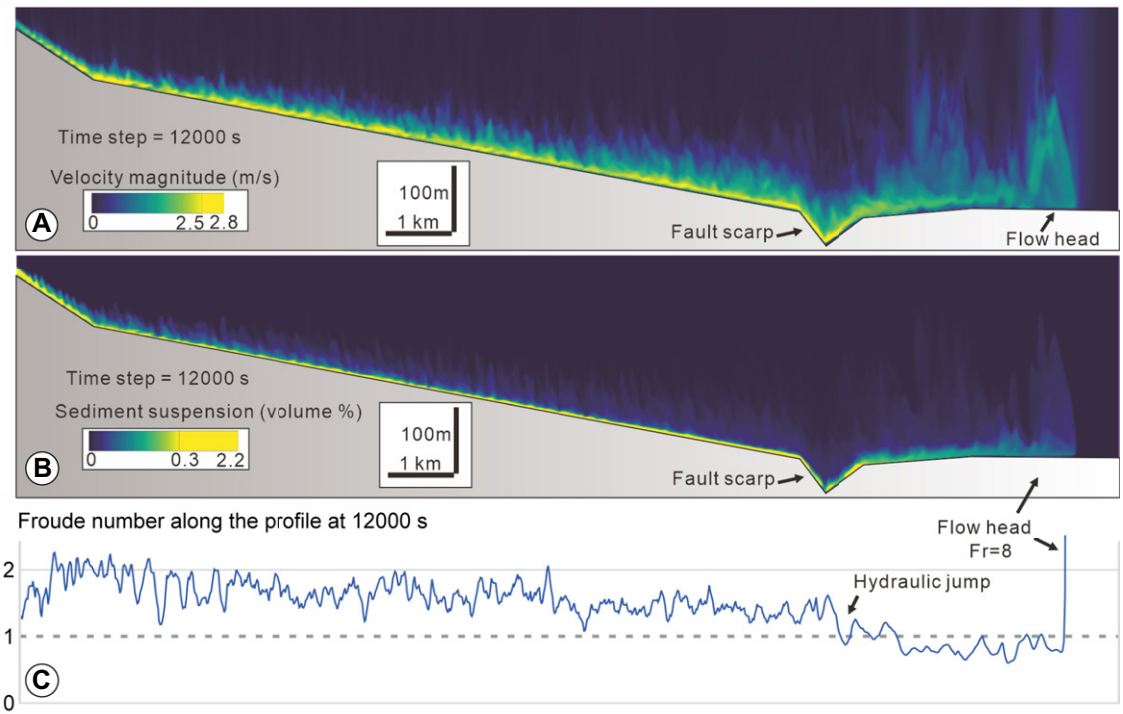

Figure 3. Modeling results for (A) velocity magnitude, (B) sediment concentration, and (C) Froude number (Fr) of a turbidity current flowing over a simplified topography. Note that the flow experiences a hydraulic jump across the fault scarp, and Fr is <1 apart from the flow head.

Chen, Q., and Sidney, S., 1997, Seismic attribute technology for reservoir forecasting and monitoring: The Leading Edge, v. 16, p. 445–448, https://doi.org/10.1190/1.1437657.

Covault, J.A., Kostic, S., Paull, C.K., Ryan, H.F., and Fildani, A., 2014, Submarine channel initiation, filling and maintenance from sea-floor geomorphology and morphodynamic modelling of cyclic steps: Sedimentology, v. 61, p. 1031–1054, https://doi.org/10.1111/sed.12084.

Covault, J.A., Kostic, S., Paull, C.K., and Sylvester, Z., 2017, Cyclic steps and related supercritical bedforms: Building blocks of deep-water depositional systems, western North America: Marine Geology, v. 393, p. 4–20, https://doi.org/10.1016/j.margeo.2016.12.009.

Elias, A., Tapponnier, P., Singh, S.C., King, G.C.P., Briais, A., Daëron, M., Carton, H., Sursock, A., Jacques, E., Jormaa, R., and Klinger, Y., 2007, Active thrusting offshore Mount Lebanon: Source of the tsunamogenic A.D. 551 Beirut-Tripoli earthquake: Geology, v. 35, p. 755–758, https://doi.org/10.1130/G23631A.1.

Ercilla, E., Wynn, R.B., Alonso, B., and Baraza, J., 2002, Initiation and evolution of turbidity current sediment waves in the Magdalena turbidite system: Marine Geology, v. 192, p. 153–169, https://doi.org/10.1016/S0025-3227(02)00553-4.

Fildani, A., Normark, W.R., Kostic, S., and Parker, G., 2006, Channel formation by flow stripping: Large-scale scour features along the Monterey East Channel and their relation to sediment waves: Sedimentology, v. 53, p. 1265–1287, https://doi.org/10.1111/j.1365-3091.2006.00812.x.

Fildani, A., Hubbard, S.M., Covault, J.A., Maier, K.L., Romans, B.W., Traer, M., and Rowland, J.C., 2013, Erosion at inception of deep-sea channels: Marine and Petroleum Geology, v. 41, p. 48–61, https://doi.org/10.1016/j.marpetgeo.2012.03.006.

Fildani, A., Kostic, S., Covault, J.A., Maier, K.L., Caress, D.W., and Paull, C.K., 2021, Exploring a new breadth of cyclic steps on distal submarine fans: Sedimentology, v. 68, p. 1378–1399, https://doi.org/10.1111/sed.12803.

Ge, Z., Nemec, W., Gawthorpe, R.L., and Hansen, E.W.M., 2017, Response of unconfined turbidity current to normal-fault topography: Sedimentology, v. 64, p. 932–959, https://doi.org/10.1111/sed.12333.

Ge, Z., Nemec, W., Gawthorpe, R.L., Rotevatn, A., and Hansen, E.W.M., 2018, Response of unconfined turbidity current to relay-ramp topography: Insights from process-based numerical modelling: Basin Research, v. 30, p. 321–343, https://doi.org/10.1111/bre.12255.

Guiastrennec-Faugas, L., Gillet, H., Jacinto, R.S., Dennielou, B., Hanquiez, V., Schmidt, S., Simplet, L., and Rousset, A., 2020, Upstream migrating knickpoints and related sedimentary processes in a submarine canyon from a rare 20-year morphobathymetric time-lapse (Capbreton submarine canyon, Bay of Biscay, France): Marine Geology, v. 423, 106143, https://doi.org/10.1016/j.margeo.2020.106143.

Heijnen, M.S., et al., 2020, Rapidly-migrating and internally-generated knickpoints can control submarine channel evolution: Nature Communications, v. 11, https://doi.org/10.1038/s41467-020-16861-x.

Howlett, D.M., Ge, Z., Nemec, W., Gawthorpe, R.L., Rotevan, A., and Jackson, C.A.-L., 2019, Response of unconfined turbidity current to deep-water fold and thrust belt topography: Orthogonal incidence on solitary and segmented folds: Sedimentology, v. 66, p. 2425–2454, https://doi.org/10.1111/sed.12602.

Jobe, Z.R., Howes, N., Romans, B.W., and Covault, J.A., 2018, Volume and recurrence of submarine-fan-building turbidity currents: The Depositional Record, v. 4, p. 160–176, https://doi.org/10.1002/dep2.42.

Kostic, S., 2011, Modeling of submarine cyclic steps: Controls on their formation, migration, and architecture: Geosphere, v. 7, p. 294–304, https://doi.org/10.1130/GES00601.1.

Maier, K.L., Brothers, D.S., Paull, C.K., McGann, M., Caress, D.W., and Conrad, J.E., 2017, Records of continental slope sediment flow morphodynamic responses to gradient and active faulting from integrated AUV and ROV data, offshore Palos Verdes, southern California Borderland: Marine Geology, v. 393, p. 47–66, https://doi.org/10.1016/j.margeo.2016.10.001.

Maier, K.L., Paull, C.K., Caress, D.W., Anderson, K., Nieminski, N.M., Lundsten, E., Erwin, B.E., Gwiazda, R., and Fildani, A., 2020, Submarine-fan development revealed by integrated high-resolution datasets from La Jolla fan, offshore California, U.S.A: Journal of Sedimentary Research, v. 90, p. 468–479, https://doi.org/10.2110/jsr.2020.22.

Maselli, V., Kneller, B., Taiwo, O.L., and Iacopini, D., 2019, Sea floor bedforms and their influence on slope accommodation: Marine and Petroleum Geology, v. 102, p. 625–637, https://doi.org/10.1016/j.marpetgeo.2019.01.021.

Meiburg, E., and Kneller, B., 2010, Turbidity currents and their deposits: Annual Review of Fluid Mechanics, v. 42, p. 135–156, https://doi.org/10.1146/annurev-fluid-121108-145618.

Menard, H.W., 1955, Deep-sea channels, topography, and sedimentation: American Association of Petroleum Geologists Bulletin, v. 39, p. 236–255.

Normandeau, A., Campbell, D.C., and Cartigny, M.J.B., 2019, The influence of turbidity currents and contour currents on the distribution of deep-water sediment waves offshore eastern Canada: Sedimentology, v. 66, p. 1746–1767, https://doi.org/10.1111/sed.12557.

Oppo, D., Evans, S., Iacopini, D., Kabir, S.M.M., Maselli, V., and Jackson, C.A.-L., 2021, Leaky salt: Pipe trails record the history of cross-evaporite fluid escape in the northern Levant Basin, Eastern Mediterranean: Basin Research, v. 33, p. 1798–1819, https://doi.org/10.1111/bre.12536.

Parker, G., and Izumi, N., 2000, Purely erosional cyclic and solitary steps created by flow over a cohesive bed: Journal of Fluid Mechanics, v. 419, p. 203–238, https://doi.org/10.1017/S0022112000001403.

Pohl, F., Eggenhuisen, J.T., Tilston, M., and Cartigny, M.J.B., 2019, New flow relaxation mechanism explains scour fields at the end of submarine channels: Nature Communications, v. 10, https://doi.org/10.1038/s41467-019-12389-x.

Postma, G., Hoyal, D.C., Abreu, V., Cartigny, M.J.B., Demko, T., Fedele, J.J., Kleverlaan, K., and Pederson, K.H., 2016, Morphodynamics of supercritical turbidity currents in the channel-lobe transition zone, *in* Lamarche, G., et al., eds., Submarine Mass Movements and Their Consequences: Dordrecht, Netherlands, Springer Science, Advances in Natural and Technological Hazards Series, v. 41, p. 469–478.

Simmons, S.M., Azpiroz-Zabala, M., Cartigny, M.J B., Clare, M.A., Cooper, C., Parsons, D.R., Pope, E.L., Sumner, E.J., and Talling, P.J., 2020, Novel acoustic method provides first detailed measurements of sediment concentration structure within submarine turbidity currents: Journal of Geophysical Research: Oceans, v. 125, https://doi.org/10.1029/2019JC015904.

Slootman, A., and Cartigny, M.J.B., 2020, Cyclic steps: Review and aggradation-based classification: Earth-Science Reviews, v. 201, https://doi.org/10.1016/j.earscirev.2019.102949.

Wynn, R.B., and Stow, D.A.V., 2002, Classification and characterisation of deep-water sediment waves: Marine Geology, v. 192, p. 7–22, https://doi.org/10.1016/S0025-3227(02)00547-9.

Zhong, G., Cartigny, M.J.B., Kuang, Z., and Wang, L., 2015, Cyclic steps along the South Taiwan Shoal and West Penghu submarine canyons on the northeastern continental slope of the South China Sea: Geological Society of America Bulletin, v. 127, p. 804–824, https://doi.org/10.1130/B31003.1.

Zhong, G., and Peng, X., 2021, Transport and accumulation of plastic litter in submarine canyons—The role of gravity flows: Geology, v. 49, p. 581–586, https://doi.org/10.1130/G48536.1.

Printed in USA